

The variance of dispersion measure of high-redshift transient objects as a probe of ionized bubble size during reionization

Shintaro Yoshiura¹[★], Keitaro Takahashi¹

¹*Department of Physics, Kumamoto University, Kumamoto, Japan*

Accepted XXX. Received YYY; in original form ZZZ

ABSTRACT

The dispersion measure (DM) of high-redshift ($z \gtrsim 6$) transient objects such as Fast Radio Bursts can be a powerful tool to probe the intergalactic medium during the Epoch of Reionization. In this paper, we study the variance of the DMs of objects with the same redshift as a potential probe of the size distribution of ionized bubbles. We calculate the DM variance with a simple model with randomly-distributed spherical bubbles. It is found that the DM variance reflects the characteristics of the probability distribution of the bubble size. We find the variance can be measured precisely enough to obtain the information on the typical size with a few hundred sources at a single redshift.

Key words: cosmology; dark ages, reionization, first stars

1 INTRODUCTION

The Epoch of Reionization (EoR) is a cosmological transition where intergalactic medium (IGM) was ionized by ionizing photons from astronomical objects in the early universe. This epoch has been observationally studied by the spectra of high- z quasars (Fan et al. 2006; McGreer et al. 2015) and the CMB optical depth (Planck Collaboration et al. 2016), which indicate the reionization was completed at $z \sim 6$ and the duration was $\Delta z < 2.7$. However, very little is known about the evolution of ionized fraction and the sources of ionizing photons.

Although first galaxies are a candidate of the ionizing source, their properties are highly uncertain. Especially, the escape fraction of ionizing photons is a key characteristic. The measured escape fraction at low redshifts ranges from 0.01 to 0.1 (Steidel et al. 2001; Iwata et al. 2009) and the predictions from numerical simulations are not necessarily consistent with differences of two orders of magnitude. Besides, star formation in galaxies, especially in low-mass galaxies, can be suppressed by feedback processes such as the photo-evaporation and photo-heating (Okamoto et al. 2008; Hasegawa & Semelin 2013), so that only heavy galaxies may have contributed to the reionization.

The topology of ionized bubbles is sensitive to the property of ionizing sources. One of powerful tools to study ionized bubbles observationally is the 21 cm line

due to hyperfine structure of hydrogen atom and the brightness temperature of the 21 cm-line signal reflects the state of IGM including the density of neutral hydrogen and spin temperature. For instance, the statistical quantities such as the power spectrum and bispectrum of the 21cm-line signal can distinguish the model of the ionizing sources (Pritchard & Furlanetto 2007; Shimabukuro et al. 2015, 2017). Beside, the topology of ionized bubbles can be directly probed by Minkowski functionals (Gleser et al. 2006; Friedrich et al. 2011; Hong et al. 2014; Yoshiura et al. 2017). However, the detection of 21 cm-line signal is highly challenging due to the presence of huge foreground.

The dispersion measure (DM) is yet another probe of the IGM during the EoR. It is defined as a line-of-sight (LOS) integration of the electron number density. An electromagnetic wave propagating through a plasma is delayed, depending on the frequency ν , with the delay time proportional to $\nu^{-2}\text{DM}$. Thus, if we can measure the DM of high-redshift transient objects, the evolution of the electron density during the EoR can be studied. In fact, previous theoretical works have reported that the DM of high-redshift Gamma Ray Bursts (GRBs) is useful to investigate reionization scenarios (Ioka 2003; Inoue 2004).

Another type of transients for the DM measurement is fast radio bursts (FRBs), which have been discovered relatively recently (Lorimer et al. 2007; Keane et al. 2011, 2012; Thornton et al. 2013; Burke-Spolaor & Bannister 2014; Spitler et al. 2014; Masui et al. 2015; Petroff et al. 2015; Ravi et al. 2015; Spitler et al. 2016; Bannister et al.

[★] E-mail: 161d9002@st.kumamoto-u.ac.jp

2017; Caleb et al. 2017; Petroff et al. 2017). As can be seen in an FRB catalog in Champion et al. (2016), FRBs generally have very large DMs, $375 < \text{DM} < 1629 \text{ pc cm}^{-3}$. Because Galactic transients typically have DMs less than 250 pc cm^{-3} , FRBs are considered to be extra-galactic events. Actually, a candidate of the host galaxy of an FRB was reported to be at $z = 0.492 \pm 0.008$ (Keane et al. 2016) although this is still under debate (Johnston et al. 2017). Very recently, Tendulkar et al. (2017) reported the host galaxy of a repeating FRB at $z \sim 0.2$.

There have been several studies on the potential of FRBs as a new cosmological probe of, for example, dark-energy (Zhou et al. 2014) and cosmological parameters (Yang & Zhang 2016) via the DM. Further, Akahori et al. (2016) found the DM and rotation measure contain information on the intergalactic magnetic field in filaments. McQuinn (2014) argued that the probability distribution of DMs reflects the amount of missing baryon surrounding halos and showed that the variance of DMs evolves with z .

In addition to these low- z studies, high- z FRBs have also been considered. For example, Zheng et al. (2014) showed that FRBs with $z \sim 3$ can be a tool to study the HeII reionization which causes the change in the differential DM, if thousands of FRBs are observed. In Fialkov & Loeb (2016), they found a relation between DM and the optical depth of the CMB suggested that the optical depth can be probed by the measurement of FRBs during EoR. If an FRB is located at $z > 6$, the DM is larger than a few thousands pc cm^{-3} . Although FRBs with such a high DM have not been observed, the observability of high- z FRBs was discussed (Fialkov & Loeb 2016, 2017). According to their estimation, the Square Kilometer Array¹ phase 2 (SKA2) can detect FRBs even at $z > 10$. Further, even the SKA phase 1 (SKA1) is expected to be able to observe bright FRBs at high redshifts Lorimer et al. (2007).

Previous works which studied the DM as a probe of reionization considered the contribution of homogeneous IGM electrons to the DM (Ioka 2003; Inoue 2004). As mentioned above, the high detection rate of FRBs is predicted based on the number density of observed FRBs (e.g. Champion et al. (2016)) and large surveys by the SKA promise the enormous detection of FRBs from EoR (Fialkov & Loeb 2016). This will give us a chance to study higher order statistics of the DM probability distribution and the inhomogeneity of IGM even at high- z . Thus, in this work, we study the effect of inhomogeneity of the IGM on the DM, considering the ionized bubbles, and introduce the variance of DMs. We discuss the potential of the DM variance to obtain information on the size distribution of ionized bubbles and estimate the necessary number of samples.

This paper is organized as follows. We introduce the dispersion measure and its variance in section 2 and our spherical bubble model in section 3. Then our primary results on the evolution of variance of dispersion measure are presented in section 4 and discuss the detectability in section 5. Finally, we conclude this paper. Through this paper we assume the Λ CDM cosmology with parameter $(\Omega_m, \Omega_\Lambda, \Omega_b, n_s, \sigma_8, H_0) = (0.31, 0.69, 0.048, 0.97, 0.82, 68 \text{ km s}^{-1} \text{ Mpc}^{-1})$ (Planck Collaboration et al. 2015).

2 DISPERSION MEASURE

The velocity of an electromagnetic wave which propagates in an ionized plasma is given as $v = c\sqrt{1 - \nu_p^2/\nu^2}$. Here, ν is the frequency, c is the speed of light and $\nu_p^2 = n_e e^2 / \pi m_e$ is the plasma frequency. Then the arrival time of the wave is delayed, compared to the case without the ionized plasma, as,

$$\Delta t = \frac{e^2}{2\pi m_e c} \frac{1}{\nu^2} \text{DM}. \quad (1)$$

Here the DM is calculated as

$$\text{DM}(z_s) = \int_0^{z_s} \frac{n_e(z)}{1+z} dl \quad (2)$$

, where n_e is the number density of free electron, the z_s is the redshift of the transient object, $dl = -cdz/(1+z)H(z)$ and $H(z) = H_0[\Omega_m(1+z)^3 + \Omega_\Lambda]^{1/2}$. Hereafter, we ignore the He reionization.

Now we consider observation of N DMs at a single redshift with various LOSs. The DM depends on the electron-density profile along the LOS, which reflects not only the evolution of average neutral fraction but its fluctuations. Previous works considered only average neutral fraction assuming a homogeneous IGM and studied the mean value of the DMs, $\overline{\text{DM}}(z) = \frac{1}{N} \sum_i^N \text{DM}_i$, as a function of redshift. In this work, we take the effect of the ionized bubble distribution into account. The electron-density profile is different for different LOSs because of the fluctuations in electron density, especially the presence of ionized bubbles. The variance of observed DMs can be estimated as, $\sigma_{\text{DM}}^2(z) = \frac{1}{N-1} \sum_i^N (\text{DM}_i - \overline{\text{DM}})^2$. It should be noted that the mean value $\overline{\text{DM}}$ is completely determined from the average neutral fraction and not affected by its inhomogeneity.

The variance of the DMs can be calculated from an integration of power spectrum of electron density as (McQuinn 2014),

$$\sigma_{\text{DM}}^2(z') \approx \int_0^{z'} \frac{cdz}{H(z)} (1+z)^{-4} n_e^2(z) \int \frac{d^2 k_\perp}{(2\pi)^2} P_k(k_\perp, z), \quad (3)$$

where $P_k(k_\perp, z)$ is the 3-dimensional spatial power spectrum of the electron number density. The power spectrum is defined by $(2\pi)^3 \delta_D(\mathbf{k} + \mathbf{k}') P_k(\mathbf{k}) = \langle \tilde{\delta}_x(\mathbf{k}) \tilde{\delta}_x(\mathbf{k}') \rangle$, where the fluctuation of x_{HII} is written as $\tilde{\delta}_x = x_{\text{HII}}/\bar{x}_{\text{HII}} - 1$, tildes denote the Fourier dual and $\langle \rangle$ indicates an ensemble average. From this expression, we see the contribution of free electrons during the EoR to the DM variance can be written as, $\sigma_{\text{DM, EoR}}^2(z) = \sigma_{\text{DM}}^2(z) - \sigma_{\text{DM}}^2(z_{\text{H}})$. Here, z_{H} is the redshift of the reionization completion and we set $z = z_{\text{H}} = 6.0$, indicated by Lyman- α absorption lines imprinted on quasars spectra.

3 SPHERICAL BUBBLE MODEL

Although numerical simulations or semi-numerical simulations (e.g. 21cmFAST (Mesinger et al. 2011)) can simulate the process of reionization and distribution of ionized bubbles, the results are often complicated and difficult to interpret. Therefore, in this work, we employ a relatively simple model of reionization taking qualitative features of (semi-)numerical simulations into account, in order to study the

¹ <https://www.skatelescope.org/>

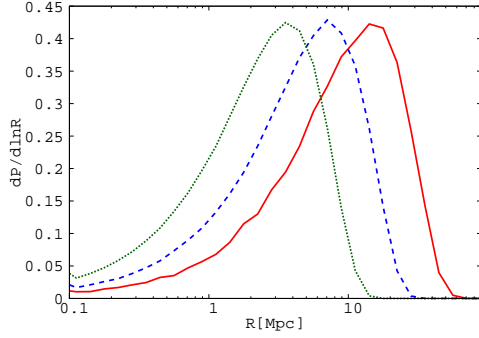


Figure 1. Probability density function of ionized bubble size for the model with $\bar{x}_{\text{HII}}=0.5$. The dashed line is our fiducial model. The solid and dotted lines are models with $R_c = 2R_{c0}$ and $R_{c0}/2$, respectively.

effect of IGM inhomogeneities on σ_{DM} and give intuitive interpretation on the results. We construct ionized bubble distribution by placing ionized bubbles spatially randomly with a probability distribution of bubble size which will be described later. The number of bubbles are tuned so that the volume-averaged neutral fraction, \bar{x}_{HII} , matches any specific value.

An important ingredient of our model is the bubble-size distribution (hereafter BSD). It has been studied both analytically (e.g. Furlanetto et al. (2004)) and numerically (e.g. Iliiev et al. (2006); Zahn et al. (2007); Kakiuchi et al. (2017); Giri et al. (2017)). These BSDs are approximately consistent with each other and can be expressed by a skewed log-normal distribution. Thus, we adopt a skewed log-normal BSD with the mean comoving radius R_c , standard deviation σ_L and skewness γ . It is expected that R_c increases, that is, ionized bubbles expand as reionization proceeds. Following Furlanetto et al. (2006), we take a fiducial model of R_c as,

$$\log R_{c0}(\bar{x}_{\text{HII}}) = 2.8\bar{x}_{\text{HII}} - 0.8. \quad (4)$$

On the other hand, σ_L and γ are assumed to be constant in time as is implied by previous works and take $\sigma_{L0}^2 = 0.3$ and $\gamma_0 = -1.7$. Fig 1 represents the examples of BSD for $\bar{x}_{\text{HII}} = 0.5$.

We do not consider partially ionized regions and assume that x_{HII} is unity inside ionized bubbles and 0 outside. This approximation is reasonable for a reionization process caused by UV photons from galaxies, because UV photons have a short mean free path and are absorbed locally to create ionized bubbles around the sources. Thus, our model would not be valid if reionization is induced mostly by X-rays, which have long mean free path. Further, we do not consider the fluctuations in the electron density within a bubble. This is a good approximation because the fluctuations in electron density are dominated by those in ionized fraction, rather than those in gas density (Shimabukuro et al. 2015)

With this model, we create free-electron density distribution of a $(1024 \text{ cMpc})^3$ box with a resolution of 512^3 . This is done at each redshift from z_{H} to 12 with a step of $\Delta z = 1$, which allows us to perform the integration of Eq. (2). These boxes with different redshifts are created independently with different seeds of random numbers. This is more reasonable compared to following the evolution of a

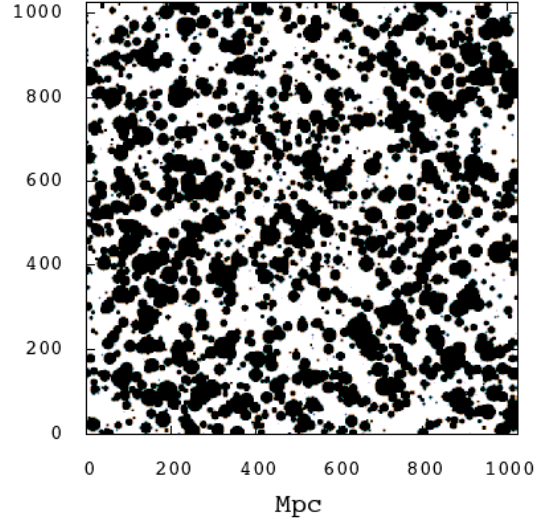


Figure 2. Slice of ionized map for fiducial model. The black represents ionized region and the length of a slice is 1024 cMpc. The ionized fraction is $\bar{x}_{\text{HII}}=0.5$.

single box in order to study the free-electron density along a light cone from a transient object. Fig. 2 represents a slice of a box for with $\bar{x}_{\text{HII}} = 0.5$. We consider two other models, varying R_c as $R_c = 2R_{c0}$ and $R_c = R_{c0}/2$, respectively, for a fixed value of \bar{x}_{HII} , to see the effect of changing the typical bubble size on σ_{DM} . For a fixed value of \bar{x}_{HII} , a small (large) R_c leads to a large (small) number of ionized bubbles. Physically, a model with a small R_c and a large number of bubbles corresponds to a case where small (low-emissivity) galaxies contribute to reionization significantly (e.g. Mesinger et al. (2016)). Because the abundance of small galaxies is determined by the effectiveness of the feedback process such as photo-evaporation and photo-heating, the parameter R_c effectively parametrizes the feedback efficiency.

4 EVOLUTION OF VARIANCE OF DISPERSION MEASURE

First, from the above simulations, we can calculate the power spectrum of the fluctuation of the free-electron density. The power spectra with $\bar{x}_{\text{HII}} = 0.3, 0.5, 0.7$ and 0.9 are plotted in the Fig. 3 for the fiducial model. The power spectra have a peak and the peak wavenumber apparently corresponds to the maximum bubble size (10.4, 36.7, 111 and 313 Mpc, respectively), for these specific realizations) rather than the mean size (1.1, 4.0, 14 and 52 Mpc, respectively). The bubble expansion is clearly seen in the shift of the peak. In spite of its simplicity, the power spectra calculated from our model reasonably agree with those from more sophisticated models (e.g. Zahn et al. (2011)).

Fig. 4 shows the power spectra with $\bar{x}_{\text{HII}} = 0.5$ with models of different R_c . The peak wavenumber shifts according to the value of R_c . Interestingly, the amplitudes of P_k are almost the same for these models and, therefore, the variances of the fluctuations in electron number density, which can be calculated as $\int d^3k P_k(k)$, are also the same.

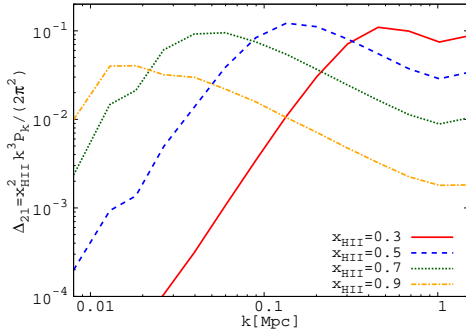


Figure 3. The power spectra for the fiducial model with several values of \bar{x}_{HII} . Solid, dashed, dotted and dot-dashed lines correspond to $\bar{x}_{\text{HII}} = 0.3, 0.5, 0.7$ and 0.9 , respectively. The mean size of ionized bubbles is $R_c = 1.1, 4.0, 14$ and 52 Mpc, respectively, while the maximum size is $10.4, 36.7, 111$ and 313 Mpc, respectively.

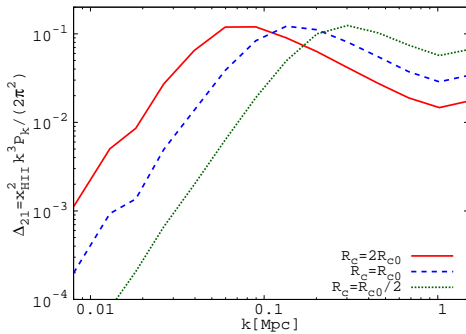


Figure 4. The power spectrum for models with $\bar{x}_{\text{HII}} = 0.5$. Solid, dashed and dotted lines have $2R_c, R_c$ and $R_c/2$, respectively.

Next, we compare the evolution of $\sigma_{\text{DM,EoR}}^2$ for the three models with different R_c , fixing the reionization history. The fiducial reionization history with $z_{\text{H}} = 6.0$ is shown as the dashed line in Fig. 5, which satisfies the observational constraints from the CMB optical depth to Thomson scattering. Since the three models have the same ionization history, they have the same value of average DM, which is shown as the thin solid line in Fig. 5. In Fig. 6, we show the evolution of $\sigma_{\text{DM,EoR}}^2$ for the three models as a function of z . We find that, as R_c increases, $\sigma_{\text{DM,EoR}}^2$ evolves more quickly. As we saw in Eq. 3, $\sigma_{\text{DM,EoR}}^2$ is obtained by a 2D integration of the 3D power spectrum. Therefore, the power spectrum which has a peak at a larger scale contributes to σ_{DM}^2 more significantly. Physically, this is understood as follows. Because a larger value of R_c leads to a sparse distribution of large bubbles, the number of bubbles which a light-ray passes is small and has a relatively large statistical fluctuations. In this case, the value of the DM strongly depends on the direction of the LOS, which leads to a large value of σ_{DM}^2 . On the other hand, for a smaller value of R_c , small bubbles are abundantly distributed so that the statistical fluctuation becomes smaller and a small value of σ_{DM}^2 is resulted.

Let us see the effect of the functional form of the BSD, which is characterized by the variance and skewness. In the top panel of Fig. 7, we compare models with $\sigma_{\text{L}}^2 = 2\sigma_{\text{L0}}^2$, σ_{L0}^2 and $\sigma_{\text{L0}}^2/2$, where $\sigma_{\text{L}}^2 = 0.3$. We find that larger variance

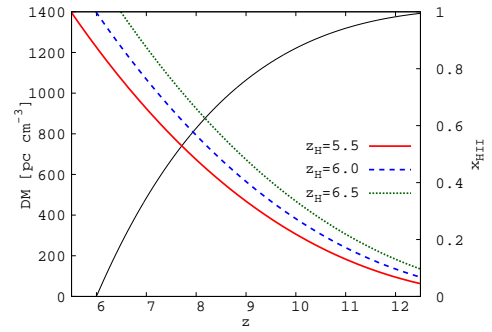


Figure 5. Thin solid line represents the redshift evolution of average dispersion measure for our fiducial ionization history ($z_{\text{H}} = 6.0$) [left vertical axis]. Other lines show the evolution of x_{HII} for $z_{\text{H}} = 5.5, 6.0$ and 6.5 [right vertical axis].

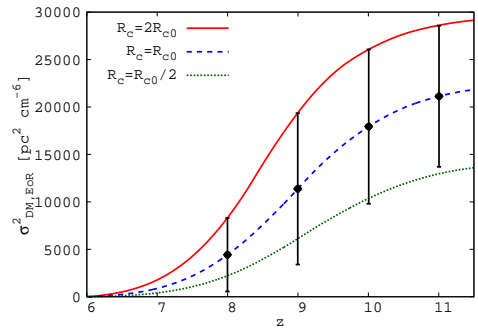


Figure 6. The redshift evolution of $\sigma_{\text{DM,EoR}}^2$ for the models with $2R_c, R_c$ and $R_c/2$. The vertical lines show the errors with the number of samples listed in Table 1 at $z = 8, 9, 10$ and 11 .

leads to a larger value of $\sigma_{\text{DM,EoR}}^2$. This is because a larger maximum bubble size is expected for a model with a larger value of variance and shifts the peak in the power spectrum to a smaller wave length (a larger scale). In addition, in the bottom panel of Fig. 7, we compare the models with $\gamma = 2\gamma_0$, γ_0 and $\gamma_0/2$, where $\gamma = -1.7$. The dependence on γ can also be understood in terms of the maximum bubble size. For a fixed mean size, the maximum size is expected to be smaller for more skewed (larger $|\gamma|$) BSD.

Finally, we study the effect of ionization history on the $\sigma_{\text{DM,EoR}}^2$. We compare three ionization models with different redshifts of reionization completion, $z_{\text{H}} = 5.5, 6.0$ and 6.5 , as shown in Fig. 5. The evolution of σ_{DM}^2 is plotted in Fig. 8. As one can see, the change of z_{H} just shifts the evolution of $\sigma_{\text{DM,EoR}}^2$. However, it should be noted that the observable σ_{DM}^2 is contributed from IGM after reionization, while Fig. 8 shows a contribution only during EoR. Therefore, the model with $z_{\text{H}} = 6.5$ has larger observable σ_{DM}^2 than other models at $z > 11$.

5 DETECTABILITY

To probe the bubble properties via $\sigma_{\text{DM,EoR}}^2$, we need to extract it from the total DM variance. Because the total DM variance is expressed as an integration from $z = 0$ to the redshift of interest, the $\sigma_{\text{DM,EoR}}^2$ is estimated as $\sigma_{\text{DM,EoR}}^2(z) =$

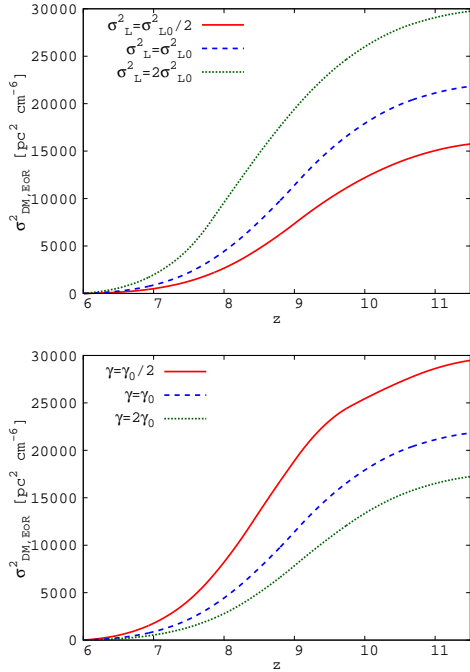


Figure 7. The redshift evolution of $\sigma_{\text{DM,EoR}}^2$ for models with different values of σ_L^2 and γ . In the top panel, solid, dashed and dotted lines have $2\sigma_{L0}^2$, σ_{L0}^2 and $\sigma_{L0}^2/2$, respectively. In the bottom panel, solid, dashed and dotted lines have $2\gamma_0$, γ_0 and $\gamma_0/2$. We assume fiducial BSD with $(\sigma_{L0}^2, \gamma_0) = (0.3, -1.7)$.

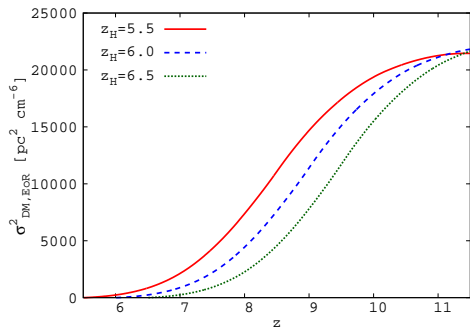


Figure 8. The redshift evolution of $\sigma_{\text{DM,EoR}}^2$ for the models with $z_H = 5.5, 6.0$ and 6.5 .

$\sigma_{\text{DM}}^2(z) - \sigma_{\text{DM}}^2(z_H)$. Thus, the DMs should be measured for the objects at the end of reionization and its variance must be estimated.

Here let us mention the DM evolution at low redshifts. McQuinn (2014) studied the mean and variance of DMs upto $z \approx 1$ considering several models of baryon distribution. It was found that the mean and variance grow rapidly from $z = 0$ to $z \sim 1$ and stay almost constant at $z \gtrsim 1$. The variance at $z \gtrsim 1$ depends on the model of baryon distribution ranging from 30,000 to 160,000. Below, we take 100,000 as a typical value.

Next, we estimate the number of FRBs necessary to obtain a useful constraint on the typical size of ionized bubbles at a single redshift. Denoting the statistical errors in $\sigma_{\text{DM}}^2(z)$ and $\sigma_{\text{DM,EoR}}^2(z)$ as $\delta(z)$ and $\delta_{\text{EoR}}(z)$, respectively, we have

Table 1. Required number of samples to distinguish models with R_c and $2R_c$.

z	8	9	10	11
$\delta_{\text{EoR}} \times 10^{-3}$	3.9	8.0	82	75
N	1450	390	420	530

$\delta_{\text{EoR}}(z) = \sqrt{(\delta(z))^2 + (\delta(z_H))^2}$. When we have N DM samples with $N \gg 1$, $\delta(z)$ is evaluated as $\sqrt{2/N}\sigma_{\text{DM}}^2(z)$. If we assume the number of samples at z_H is much larger than that at the redshift of interest ($z > z_H$), $\delta(z_H)$ can be neglected and we have $\delta_{\text{EoR}}(z) \sim \delta(z)$. Considering a nominal redshift $z = 9$, the typical values of $\sigma_{\text{DM}}^2(z)$ and $\sigma_{\text{DM,EoR}}^2(z)$ are 100,000 and 11,000 (see Fig. 6), respectively. To distinguish our fiducial model and a model with $R_c = 2R_{c0}$, we need an accuracy of about 8,000 so that the minimum necessary number of samples is estimated to be 400. In the same way, we evaluate the number of samples required for distinguishing the models with R_c and $2R_c$ at four redshifts. We tabulate them in Table 5 and show the errors as vertical lines in Fig. 6.

Here we ignored the DMs contributed from the Milky Way and the host galaxy of FRBs. According to Dolag et al. (2015), the disc and spiral arm of the Milky Way contribute to the DM by less than few hundreds pc cm⁻³ except galactic center and the contribution from the galactic halo is about 30 pc cm⁻³. Thus, they are expected to be negligible for our purpose.

The existence of FRBs during EoR is of critical importance in our method and it is deeply related to the origin of FRBs. Although the origin itself is outside the scope of this paper, let us mention the possibility of detecting such FRBs with the SKA in future. So far, while the FRB reported in Champion et al. (2016) has a large DM \sim 1600 indicating it is located at $z > 1$, we have no evidence of the existence of FRBs at such high redshifts ($z \gtrsim 6$). Nevertheless, in Fialkov & Loeb (2016), they showed that, assuming the observation time of 100 ms for SKA_LOW and 1ms for SKA_MID, FRBs at $z = 10$ with a peak luminosity as large as 5×10^{33} [erg s⁻¹ Hz⁻¹ sr⁻¹] found in Masui et al. (2015) can be detected by SKA1. Besides, the high detection rate is also crucial in our method. Recently, Champion et al. (2016); Lawrence et al. (2016); Rane et al. (2016) estimated the detection rate of FRBs with flux density 1 Jy ms to be 2×10^3 per sky per day at $z < 1$. Based on the estimation, Fialkov & Loeb (2017) found the detection rate, 6000 [sky⁻¹ day⁻¹] from the EoR, as observed by SKA2_MID. Thus, considering that FRB search with the SKA will be performed as a commensal observation with pulsar search, there is a possibility for the detection of a relatively large number of FRBs at EoR, required by our method.

6 SUMMARY AND DISCUSSION

In this paper, we studied the effect of ionized bubbles on the DM variance of objects during the Epoch of Reionization. The mean DM and the variance were calculated by using a simple model of spherical ionized bubbles with a reasonable size distribution implied by more sophisticated models. We

found that the DM variance is sensitive to the probability distribution of bubble size and can be used to probe it. Then the statistical error of the variance was evaluated and the number of sources necessary to obtain useful information is estimated to be about several hundreds to 1,000 at a single redshift. Because the bubble size reflects the abundance of ionizing sources and their emissivity, the DM variance can be a powerful tool to probe the type of ionizing source. Even if only a very small fraction of observed FRBs are located at high redshifts, detection of several hundreds of FRBs would be possible with an unprecedented survey of the SKA, although follow-up observations to determine the redshift of the host galaxy is necessary.

We focused on objects which emit UV photons such as star forming galaxies. They are regarded as a primary candidate of ionizing sources during the EoR. However, if quasars are main sources, the distribution of free electrons would be very different from the one considered here, because quasars emit X-rays which have much larger mean free paths compared to UV photons. Then, the power spectrum is larger at large scales since the typical bubble size is enhanced (Kulkarni et al. 2017) and, thus, the σ_{DM} becomes large.

As discussed above, the measurement of $\sigma_{\text{DM,EoR}}$ can probe the BSD and then we can interpret the result as the property of ionizing sources. For example, a small value of $\sigma_{\text{DM,EoR}}$ indicates that there are many ionizing sources with low ionizing efficiency which provide small bubbles. This suggests, for example, that weak feedback effect allows small halo to make stars and the escape fraction of heavy galaxy is low. Thus, the observation of σ_{DM} could become a powerful tool to probe these early objects and is complementary to 21cm-line observations.

ACKNOWLEDGEMENT

We are grateful to Dr. H. Shimabukuro for helpful comments on a draft version of this manuscript. This work is supported by Grant-in-Aid from the Ministry of Education, Culture, Sports, Science and Technology (MEXT) of Japan, Nos. 24340048, 26610048, 15H05896, 16H05999, 17H01110 (K.T.) and 16J01585 (S.Y.), and Bilateral Joint Research Projects of JSPS (K.T.).

REFERENCES

- Akahori, T., Ryu, D., & Gaensler, B. M. 2016, *ApJ*, 824, 105
 Burke-Spolaor, S., & Bannister, K. W. 2014, *ApJ*, 792, 19
 Bannister, K. W., Shannon, R. M., Macquart, J.-P., et al. 2017, *ApJ*, 841, L12
 Caleb, M., Flynn, C., Bailes, M., et al. 2017, *MNRAS*, 468, 3746
 Champion, D. J., Petroff, E., Kramer, M., et al. 2016, *MNRAS*, 460, L30
 Dolag, K., Gaensler, B. M., Beck, A. M., & Beck, M. C. 2015, *MNRAS*, 451, 4277
 Fan, X., Strauss, M. A., Becker, R. H., et al. 2006, *AJ*, 132, 117
 Fialkov, A., & Loeb, A. 2016, *J. Cosmology Astropart. Phys.*, 5, 004
 Fialkov, A., & Loeb, A. 2017, arXiv:1706.06582
 Furlanetto, S. R., Zaldarriaga, M., & Hernquist, L. 2004, *ApJ*, 613, 1
 Furlanetto, S. R., & Oh, S. P. 2005, *MNRAS*, 363, 1031
 Furlanetto, S. R., McQuinn, M., & Hernquist, L. 2006, *MNRAS*, 365, 115
 Friedrich, M. M., Mellema, G., Alvarez, M. A., Shapiro, P. R., & Iliev, I. T. 2011, *MNRAS*, 413, 1353
 Giri, S. K., Mellema, G., Dixon, K. L., & Iliev, I. T. 2017, arXiv:1706.00665
 Gleser, L., Nusser, A., Ciardi, B., & Desjacques, V. 2006, *MNRAS*, 370, 1329
 Hasegawa, K., & Semelin, B. 2013, *MNRAS*, 428, 154
 Hong, S. E., Ahn, K., Park, C., et al. 2014, *Journal of Korean Astronomical Society*, 47, 49
 Iliev, I. T., Mellema, G., Pen, U.-L., et al. 2006, *MNRAS*, 369, 1625
 Inoue, S. 2004, *MNRAS*, 348, 999
 Ioka, K. 2003, *ApJ*, 598, L79
 Iwata, et al. 2009, *ApJ*, 692, 1287
 Johnston, S., Keane, E. F., Bhandari, S., et al. 2017, *MNRAS*, 465, 2143
 Kakiichi, K., Majumdar, S., Mellema, G., et al. 2017, arXiv:1702.02520
 Keane, E. F., Kramer, M., Lyne, A. G., Stappers, B. W., & McLaughlin, M. A. 2011, *MNRAS*, 415, 3065
 Keane, E. F., Stappers, B. W., Kramer, M., & Lyne, A. G. 2012, *MNRAS*, 425, L71
 Keane, E. F., Johnston, S., Bhandari, S., et al. 2016, *Nature*, 530, 453
 Kulkarni, G., Choudhury, T. R., Puchwein, E., & Haehnelt, M. G. 2017, arXiv:1701.04408
 Lawrence, E., Vander Wiel, S., Law, C. J., Burke Spolaor, S., & Bower, G. C. 2016, arXiv:1611.00458
 Lorimer, D. R., Bailes, M., McLaughlin, M. A., Narkevic, D. J., & Crawford, F. 2007, *Science*, 318, 777
 Lorimer, D. R., Karastergiou, A., McLaughlin, M. A., & Johnston, S. 2013, *MNRAS*, 436, L5
 Masui, K., Lin, H.-H., Sievers, J., et al. 2015, *Nature*, 528, 523
 McGreer, I. D., Mesinger, A., & D’Odorico, V. 2015, *MNRAS*, 447, 499
 McQuinn, M. 2014, *ApJ*, 780, L33
 Mesinger, A., Furlanetto, S., & Cen, R. 2011, *MNRAS*, 411, 955
 Mesinger, A., Greig, B., & Sobacchi, E. 2016, *MNRAS*, 459, 2342
 Okamoto, T., Gao, L., & Theuns, T. 2008, *MNRAS*, 390, 920
 Petroff, E., Bailes, M., Barr, E. D., et al. 2015, *MNRAS*, 447, 246
 Petroff, E., Burke-Spolaor, S., Keane, E. F., et al. 2017, *MNRAS*, 469, 4465
 Planck Collaboration, Ade, P. A. R., Aghanim, N., et al. 2015, arXiv:1502.01589
 Planck Collaboration, Adam, R., Aghanim, N., et al. 2016, *A&A*, 596, A108
 Pritchard, J. R., & Furlanetto, S. R. 2007, *MNRAS*, 376, 1680
 Ravi, V., Shannon, R. M., & Jameson, A. 2015, *ApJ*, 799, L5
 Rane, A., Lorimer, D. R., Bates, S. D., et al. 2016, *MNRAS*, 455, 2207
 Shimabukuro, H., Yoshiura, S., Takahashi, K., Yokoyama, S., & Ichiki, K. 2015, *MNRAS*, 451, 467
 Shimabukuro, H., Yoshiura, S., Takahashi, K., Yokoyama, S., & Ichiki, K. 2017, *MNRAS*, 468, 1542
 Spitler, L. G., Cordes, J. M., Hessels, J. W. T., et al. 2014, *ApJ*, 790, 101
 Spitler, L. G., Scholz, P., Hessels, J. W. T., et al. 2016, *Nature*, 531, 202
 Steidel, C. C., Pettini, M., Adelberger, K. L. 2001, *ApJ*, 546, 665
 Tendulkar, S. P., Bassa, C., Cordes, J. M., et al. 2017, arXiv:1701.01100
 Thornton, D., Stappers, B., Bailes, M., et al. 2013, *Science*, 341, 53
 Totani, T. 2013, *PASJ*, 65,
 Yoshiura, S., Shimabukuro, H., Takahashi, K., & Matsubara, T. 2017, *MNRAS*, 465, 394

- Zahn, O., Lidz, A., McQuinn, M., et al. 2007, ApJ, 654, 12
Zahn, O., Mesinger, A., McQuinn, M., et al. 2011, MNRAS, 414,
727
Yang, Y.-P., & Zhang, B. 2016, ApJ, 830, L31
Zheng, Z., Ofek, E. O., Kulkarni, S. R., Neill, J. D., & Juric, M.
2014, ApJ, 797, 71
Zhou, B., Li, X., Wang, T., Fan, Y.-Z., & Wei, D.-M. 2014, Phys.
Rev. D, 89, 107303

This paper has been typeset from a $\text{\TeX}/\text{\LaTeX}$ file prepared by
the author.